RSC Advances

PAPER

View Article Online
View Journal | View Issue

Cite this: *RSC Adv.*, 2022, **12**, 7446

Effect of hydrophilic block end groups and block junction on block copolymer self-assembly in solution†

Sungmin Ha and Kyoung Taek Kim *

Recent research suggests that the end groups of polymers can affect their self-assembly. However, the effect of end groups on the self-assembly of block copolymers in solution remains unclear, and thus far, only micelle–vesicle transformations have been achieved *via* end-group modification. Herein, we report that hydrophilic block end groups and the junction between two blocks can affect the solution self-assembly of block copolymers, leading to the formation of different morphologies, including vesicles, cubosomes, and hexosomes. Poly(ethylene glycol)-*b*-polystyrene (PEG-*b*-PS) with hydroxyl, methoxy, azido, or amino groups at the PEG chain ends was synthesized and self-assembled in solution *via* the cosolvent method. As a result, the morphology of the block copolymers transformed from vesicles to hexosomes upon increasing the end-group hydrophobicity. In addition, a morphological transition from cubosomes to vesicles was observed upon changing the junction from a triazole to an amide, and the interaction between the solvent and end groups significantly affected the self-assembly behavior.

Received 24th January 2022
Accepted 1st March 2022

DOI: 10.1039/d2ra00493c

rsc.li/rsc-advances

1. Introduction

Amphiphilic block copolymers (ABCPs) self-assemble in solution to form various morphologies such as micelles, vesicles,[1–5] cubosomes,[6–19] and hexosomes.[10,11,20–28] The chemical structure, block ratio, and molecular weight distribution of ABCPs influence their self-assembly.[4,18,29,30] In addition, recent studies have shown that the end groups of polymers, despite only accounting for small mass and volume fractions of an entire polymer, could affect or induce polymer self-assembly. The end group effect was first investigated in the self-assembly of hydrophilic homopolymers.[31–33] Xu *et al.* synthesized hydrophilic homo- and copolymers with two hydrophobic pyrene or cholesterol groups at the ω-terminus.[31] The polymers self-assembled to form polymer vesicles, and it was demonstrated that the two rigid hydrophobic end groups were responsible for the vesicle formation. O'Reilly and co-workers observed unusual micelle formation by the self-assembly of hydrophilic homopolymers with hydrophobic end groups at both ends.[32] They synthesized a series of hydrophilic homopolymers with a pyrene and a dodecyl carbonotrithiocarbonate group at each end *via* reversible addition–fragmentation chain transfer (RAFT) polymerization. The homopolymers with the hydrophobic groups at both ends self-assembled in an acidic aqueous solution to form well-defined aggregated micelles that behaved similarly to ABA′ block copolymers. Liu *et al.* demonstrated that the terminal alkyne group of hydrophilic homopolymers could drive the polymer self-assembly into vesicles and flower-like complex particles.[33] They prepared a series of differently end-functionalized hydrophilic homopolymers *via* atom transfer radical polymerization (ATRP). During self-assembly in aqueous solution, only the homopolymers with terminal alkyne groups formed various morphologies including spherical micelles, multicompartment vesicles, and flower-like complex particles. The authors suggest that intermolecular hydrogen bonding between the terminal protons of the alkyne groups and oxygen atoms of the carbonyl groups drives the self-assembly.

The effect of end groups on block copolymer self-assembly has been investigated mostly based on bulk self-assembly[34–37] or polymerization-induced self-assembly (PISA).[38,39] Park and co-workers investigated the effect of the end groups of PEG blocks on the self-assembled morphology of PS-*b*-PEG along with other properties including conductivity and ion transport properties.[34–37] They observed the formation of a disordered phase from hydroxyl-terminated PEG-*b*-PS while sulfonate-terminated PEG-*b*-PS formed lamellar, hexagonal, and gyroid phases depending on the concentration of lithium salt added during the self-assembly.[34] Blackman *et al.* compared the photo- and thermally initiated PISA behaviors of poly(ethylene glycol)-*b*-(2-hydroxypropyl methacrylate).[38] They found that photo-initiated PISA produced higher-order structures owing to the loss of the end group during the process. In addition, extended irradiation of light or heat could induce a worm-to-vesicle morphological transition. Davis and co-workers reported that

Department of Chemistry, Seoul National University, Seoul 08826, Republic of Korea. E-mail: ktkim72@snu.ac.kr

† Electronic supplementary information (ESI) available: Experimental details including synthetic procedures, characterization, and spectroscopy data. See DOI: 10.1039/d2ra00493c

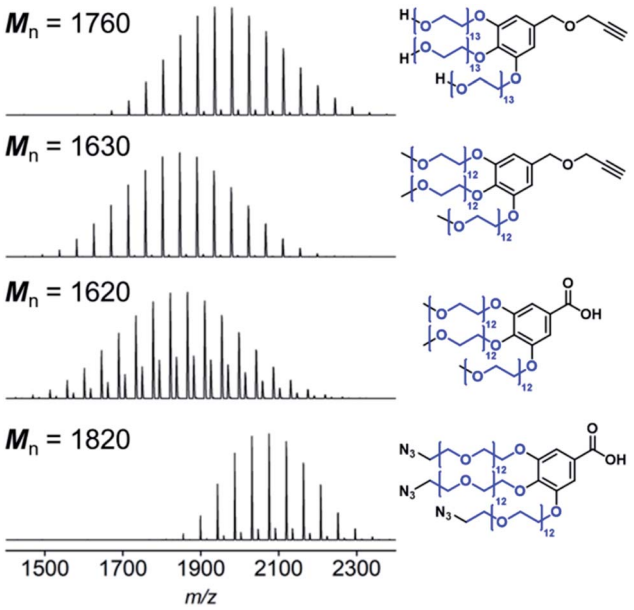

Fig. 1 MALDI-TOF spectra of the PEG blocks. M_n of the PEG chains (shown in blue) was calculated from the spectra (Table S1†).

vesicle formation could be induced from a micelle-forming PISA system by increasing the RAFT end-group hydrophobicity of the macromolecular chain transfer agent (macro-CTA).[39] They prepared two hydrophilic macro-CTAs with a carboxylic acid or a methyl ester end group and compared the PISA morphologies after the RAFT aqueous emulsion polymerization of styrene. Consequently, the methyl-ester-terminated block copolymer formed vesicles, whereas the carboxyl-terminated one formed micelles. With regard to self-assembly using the film hydration method, Grzelakowski and Kita-Tokarczyk synthesized a series of ABA or BA block copolymers comprising poly(2-methyloxazoline) (PMOXA) and poly(dimethylsiloxane) (PDMS) with different functional groups at both ends.[40] Notably, while the ABA block copolymer with hydroxyl groups at both ends formed micelles, the block copolymer self-assembled into vesicles after methacrylation of the hydroxyl groups despite a low conversion (*ca.* 5%) of the methacrylation. According to the authors, the morphological transition could be attributed to the difference between the hydroxyl and methacryl groups in terms of size, dipole moment, and polarizability.

Recently, Che *et al.* reported a morphological transition of azide-modified PEG-*b*-PS (N_3-PEG-*b*-PS) vesicles into hexagonally packed hollow hoops (HHHs) induced by osmotic pressure during dialysis against NaCl solution.[41] In contrast, vesicles of PEG-*b*-PS with a methoxy end group (mPEG-*b*-PS) deformed into stomatocytes. The authors suggest that azide coordination to water molecules increases the hydrodynamic volume of the PEG at the internal side of the vesicles, compared to the PEG volume at the external side, leading to the formation of HHHs.

Most studies on the effect of end groups on block copolymer self-assembly have focused on the morphological transition between micelles and vesicles. The effect of end groups on inverse-phase-forming block copolymers has rarely been studied. Herein, we investigated the influence of the end groups of the hydrophilic block on inverse-phase-forming block copolymer self-assembly in solution. Additionally, we report that the junction between two blocks can affect the solution self-assembly of block copolymers. First, branched PEG hydrophilic blocks with methoxy, hydroxyl, or azido groups at the PEG chain ends were synthesized and coupled with PSs *via* copper-catalyzed azide–alkyne cycloadditions (CuAAC) or amidation. PEG-*b*-PS with amino end groups was obtained *via* reduction of the PEG-PE with azido groups. Block copolymers with different

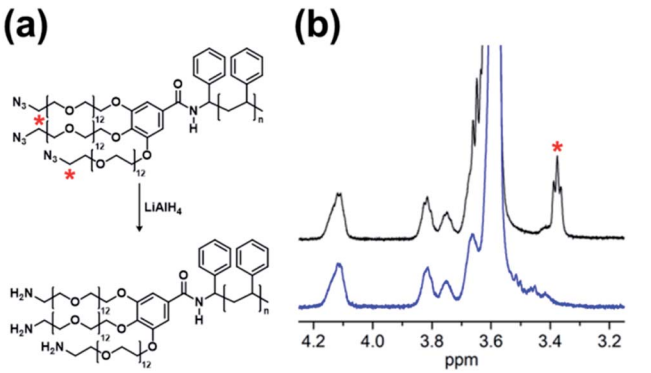

Fig. 3 (a) Reduction scheme of $(N_3\text{-PEG})_3$-amd-PS1. (b) NMR spectra (right) of $(N_3\text{-PEG})_3$-amd-PS1 (black) and $(H_2N\text{-PEG})_3$-amd-PS1 (blue).

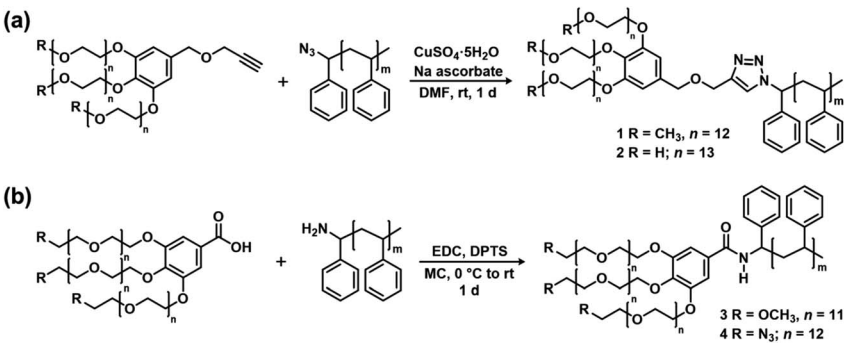

Fig. 2 Synthesis of the block copolymers with different end groups and junctions *via* (a) CuAAC and (b) amidation.

Table 1 Gel permeation chromatography (GPC) profiles of PS and block copolymers (BCPs)

BCP	M_n (PEG)[a] (g mol^{-1})	M_n (PS)[b] (g mol^{-1})	M_n (BCP)[b] (g mol^{-1})	$Đ$[b] (BCP)	w_{PEG} (wt%)
(HO-PEG)$_3$-trz-PS**1**	1760	16 900	20 200	1.09	10.4
(MeO-PEG)$_3$-trz-PS**2**	1630	15 300	18 700	1.09	10.7
(MeO-PEG)$_3$-amd-PS**2**	1620	15 300	18 900	1.05	10.6
(N$_3$-PEG)$_3$-amd-PS**1**	1820	16 900	20 000	1.05	10.8
(H$_2$N-PEG)$_3$-amd-PS**1**	1820	16 900	19 700	1.07	10.8

[a] M_n (PEG) was calculated from the MALDI-TOF spectra of each PEG block. [b] M_n (PS) (M_n of PS), M_n (BCP) (M_n of a block copolymer), and $Đ$ (BCP) (dispersity of a block copolymer) were determined by GPC (DMF, 35 °C, 1 mL min^{-1}) using PS standards.

end groups were self-assembled in solution *via* the cosolvent method to demonstrate the effect of the end groups on the self-assembled morphologies.[4] In addition, the variation in morphological changes in response to a solvent change from dioxane to acetone was studied based on the block copolymers with different end groups.

2. Results and discussion

Synthesis of PEG-*b*-PS with different end groups

Starting from PEG monomethyl ether or PEG diol, we synthesized hydrophilic blocks with three PEG branches end-functionalized with methoxy, hydroxyl, and azido groups (Fig. S1†). Hydroxyl PEG block with an alkyne group at the other end was synthesized according to our previous study.[13] Methoxy PEG blocks with an alkyne group or a carboxyl group were synthesized by tethering α-methoxy-ω-tosyl PEGs to a methyl gallate, which was followed by hydrolysis or reduction and subsequent etherification with a propargyl bromide to introduce carboxyl or alkyne group for conjugation with PS. Azido PEG block with a carboxyl group was prepared from α-azido-ω-tosyl PEG in the same way. Synthesis of the hydrophilic blocks was confirmed by MALDI-TOF mass spectrometry and NMR spectroscopy (Table S1,† Fig. 1 and S2–S5†).

Two different PSs, PS**1** (M_n = 16 900 g mol^{-1}) and PS**2** (M_n = 15 300 g mol^{-1}), were obtained by ATRP. Their molecular weights were adjusted such that the block copolymers had a similar block ratio (w_{PEG}), which was calculated as the ratio of the M_n of the PEG block to that of the PS block (Table 1 and S1†). The terminal bromo group of the PSs was converted into an azido group or an amino group for conjugation with the PEG blocks according to a previous study.[42]

The PEG blocks and the PS were coupled *via* CuAAC (Fig. 2a) or amidation (Fig. 2b) to obtain hydroxyl, methoxy, and azido PEG-*b*-PSs with a triazole (denoted "trz") or an amide bond (denoted "amd") linking the two blocks. The azido PEG-*b*-PS was further reduced to obtain the amino PEG-*b*-PS, (H$_2$N-PEG)$_3$-amd-PS**1** and the conversion was confirmed by the disappearance of the NMR proton peak for the carbon adjacent to the azido group (Fig. 3). As a result, we prepared five block copolymers with different end groups and junctions but similar block ratios, as confirmed by GPC and NMR analysis (Table 1, Fig. 4 and S6–S10†).

Self-assembly of the block copolymers in solution

The block copolymers were self-assembled *via* the cosolvent method using acetone or dioxane, which are common solvents, as previously described.[13] A block copolymer was dissolved in a common solvent and self-assembly was induced by slowly adding the same volume of water. We observed a wide range of morphologies from vesicles to hexosomes depending on the different end groups and junctions.

(HO-PEG)$_3$-trz-PS**1** formed vesicles in dioxane (Fig. 5b), whereas a mixture of spongesomes and cubosomes was formed in acetone (Fig. 5a and S11c†). As previously reported, the PS chain is assumed to have a reduced critical chain length (l_c) owing to its lower solubility in acetone than in dioxane, leading to the formation of morphologies with a higher packing parameter ($p = V/a_0 l_c$).[13] Under the same self-assembly conditions, (MeO-PEG)$_3$-trz-PS**2** self-assembled into cubosomes in both solvents (Fig. 5c, d, S11a and b†). Considering that the l_c in dioxane is greater than in acetone, the hydrophilic headgroup area (a_0) of (MeO-PEG)$_3$-trz-PS**2** should be smaller in dioxane than in acetone to compensate for the difference in l_c.

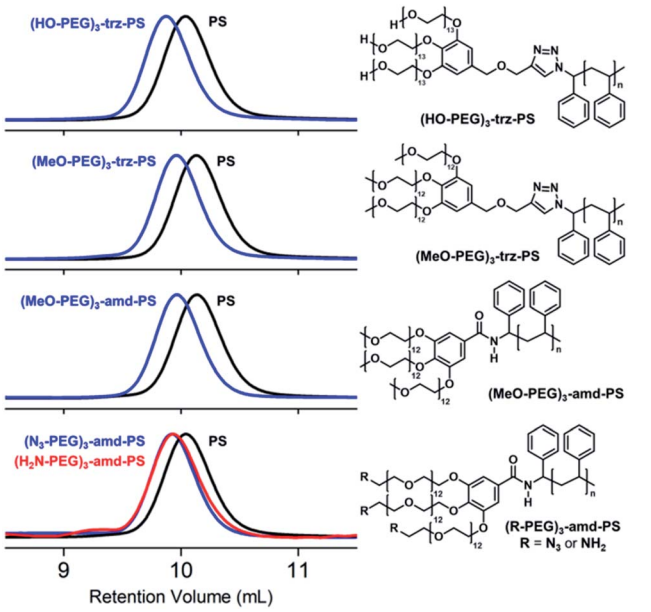

Fig. 4 GPC chromatograms (left) and chemical structures (right) of the BCPs. In the GPC chromatograms, PSs are shown in black and BCPs are shown in blue or red.

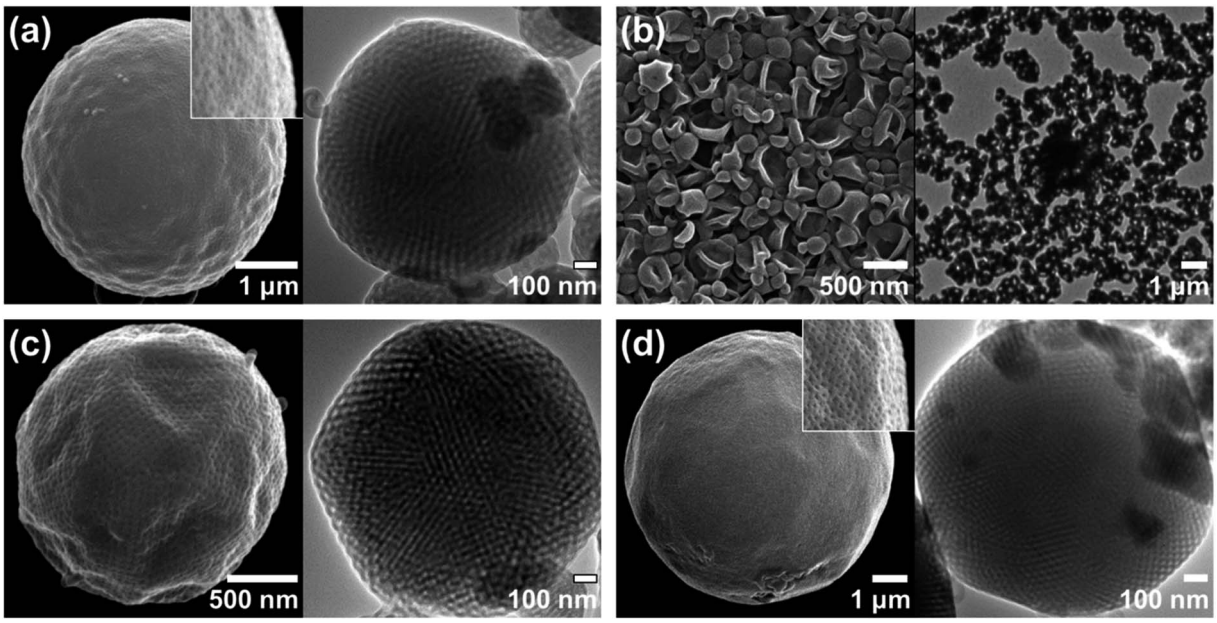

Fig. 5 Representative SEM and TEM images of (a and b) (HO-PEG)$_3$-trz-PS**1** self-assembled in (a) acetone (cubosomes and spongesomes) and (b) dioxane (vesicles), and (c and d) (MeO-PEG)$_3$-trz-PS**2** in (c) acetone (cubosomes) and (d) dioxane (cubosomes).

Moreover, it can be inferred that the a_0 value is larger for (HO-PEG)$_3$-trz-PS**1** than for (MeO-PEG)$_3$-trz-PS**2** in both solvents, possibly owing to the higher hydrophilicity of the hydroxyl group compared to that of the methoxy group. These results are consistent with those of the previous study by Davis and co-workers that revealed micelle–vesicle transformations with an

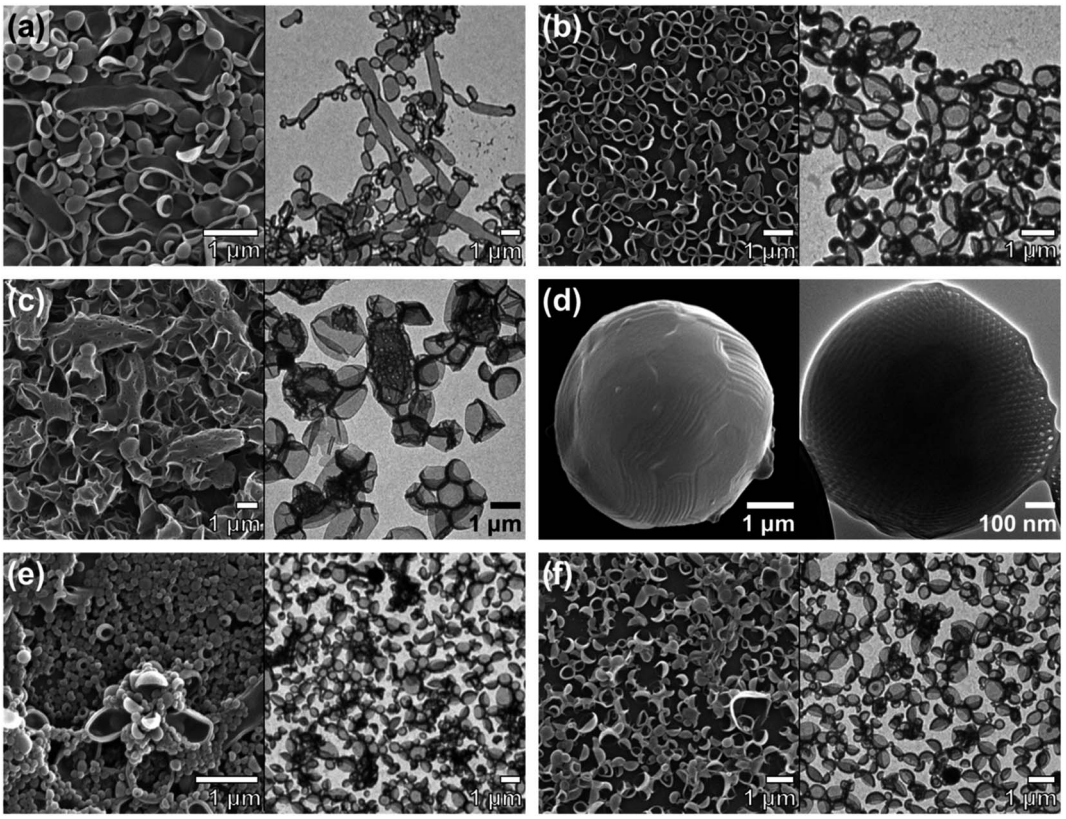

Fig. 6 Representative SEM and TEM images of (a and b) (MeO-PEG)$_3$-amd-PS**2** self-assembled in (a) acetone (vesicles and lamellae) and (b) dioxane (vesicles), (c and d) (N$_3$-PEG)$_3$-amd-PS**1** in (c) acetone (vesicles and sponges) and (d) dioxane (hexosomes), and (e and f) (H$_2$N-PEG)$_3$-amd-PS**1** in (e) acetone (vesicles) and (d) dioxane (vesicles).

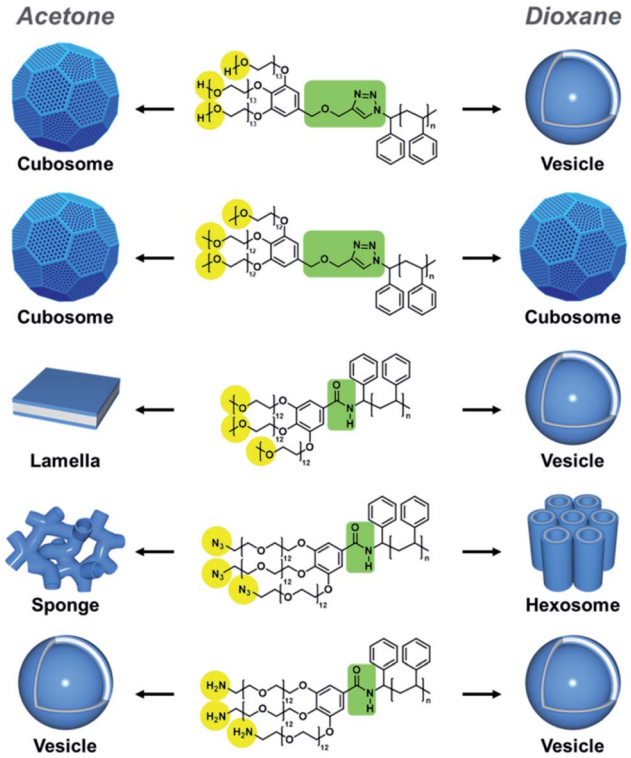

Fig. 7 Schematic representation of BCP self-assembly showing major morphologies self-assembled in acetone (left) and dioxane (right).

increasing packing parameter upon increasing the end-group hydrophobicity.[39] The hydroxyl and methoxy end groups directly affect the BCP self-assembly by varying the a_0 due to their different interactions with water and the common solvent.

To further investigate the effect of azido and amino end groups, we compared the self-assembly of (MeO-PEG)$_3$-amd-PS**2**, (N$_3$-PEG)$_3$-amd-PS**1**, and (H$_2$N-PEG)$_3$-amd-PS**1** (Fig. 6 and 7). (MeO-PEG)$_3$-amd-PS**2** and (N$_3$-PEG)$_3$-amd-PS**1** self-assembled in acetone to form a mixture of lamellae and vesicles or a mixture of sponges and vesicles, respectively (Fig. 6a and c). Interestingly, (N$_3$-PEG)$_3$-amd-PS**1** self-assembled into hexosomes in acetone (Fig. 6d and S11d†) while (MeO-PEG)$_3$-amd-PS**2** only formed vesicles (Fig. 6b). This substantial difference in morphologies in terms of the packing parameter may arise from the higher hydrophobicity of azido PEGs. Hartwig and co-workers reported that the conversion of a hydrogen to an azide in cycloheximide and digoxigenin derivatives increased their distribution coefficient values.[43] Therefore, the azido PEG should have higher hydrophobicity than that of the methoxy PEG.[44–46] Specifically, (N$_3$-PEG)$_3$-amd-PS**1** should possess a significantly smaller a_0 value than that of vesicle-forming (MeO-PEG)$_3$-amd-PS**2**, leading to high-packing-parameter hexosome formation in dioxane. Moreover, it can be inferred that (N$_3$-PEG)$_3$-amd-PS**1** should possess a much smaller a_0 value in dioxane than that in acetone to increase the packing parameter while the l_c of PS decreases. Meanwhile, only vesicles were observed from the self-assembly of (H$_2$N-PEG)$_3$-amd-PS**1** in both solvents owing to the high hydrophilicity of the amino groups.[43]

Remarkably, we found that the junction between the two blocks could also affect the BCP self-assembly. In both solvents, (MeO-PEG)$_3$-trz-PS**2** and (MeO-PEG)$_3$-amd-PS**2** self-assembled into cubosomes and mainly vesicles, respectively (Fig. 5c, d, S11a, b, S6a, and b†). Owing to the methoxy end groups, both BCPs exhibited small morphological changes upon varying the solvent from acetone to dioxane; this is due to the decrease in a_0 offsetting the increase in l_c. An amide unit can act both as a strong hydrogen-bonding donor and an acceptor, whereas a 1,2,3-triazole unit is a weak hydrogen bonding acceptor.[47,48] Therefore, the hydrogen bonding between the amide bond in (MeO-PEG)$_3$-amd-PS**2** and other amide junctions or water molecules could affect the BCP conformation. The difference in the length of the junction between (MeO-PEG)$_3$-trz-PS**2** and (MeO-PEG)$_3$-amd-PS**2** could be another factor.

Based on the aforementioned reasons, (MeO-PEG)$_3$-amd-PS**2** may possess a larger a_0 value than that of (MeO-PEG)$_3$-trz-PS**2**, leading to vesicle formation, whereas (MeO-PEG)$_3$-trz-PS**2** forms cubosomes under the same self-assembly conditions. Moreover, the effect of hydrogen-bonding-forming units on the self-assembly process has been studied based on the supramolecular self-assembly of low-molecular-weight π-amphiphiles.[49–53] Considering the differences in the self-assembly behaviors of (MeO-PEG)$_3$-amd-PS**2** and (MeO-PEG)$_3$-trz-PS**2**, we suggest that a small difference in the junction could affect the self-assembly of high-molecular-weight BCPs. Regarding the effect of the junction, Hawker and co-workers previously demonstrated that the phase separation strength of a BCP could be increased by ionization of its triazole junction, which leads to electrostatic interactions between counterions of adjacent domain junctions.[54] The self-assembly behavior with respect to the end groups and the junction is summarized in Table 2 and Fig. 7 for each common solvent.

Table 2 Summary of self-assembled morphologies in acetone and dioxane

	Self-assembled morphology			
BCP	Acetone	Dioxane	End group hydrophilicity	Junction
(HO-PEG)$_3$-trz-PS**1**	Cubosome spongesome	Vesicle	Hydrophilic	Triazole
(MeO-PEG)$_3$-trz-PS**2**	Cubosome	Cubosome	Hydrophobic	Triazole
(MeO-PEG)$_3$-amd-PS**2**	Lamella, vesicle	Vesicle	Hydrophobic	Amide
(N$_3$-PEG)$_3$-amd-PS**1**	Sponge, vesicle	Hexosome	Hydrophobic	Amide
(H$_2$N-PEG)$_3$-amd-PS**1**	Vesicle	Vesicle	Hydrophilic	Amide

From the thermodynamic aspect, BCP self-assembly in solution relies on interfacial energy, which is determined by solvent affinity and block composition of the BCP.[46,55] In the cosolvent method, the self-assembled morphology of a BCP depends on the affinity of the blocks to a solvent mixture of water and the common solvent. Considering the effect of the core-block hydrophobicity on BCP self-assembly,[44–46] hydrophilicity of the corona block should also influence the self-assembled morphologies of the BCP. According to our findings, different end groups strongly affect the hydrophilicity of the corona block, thus leading to significant changes in self-assembled morphologies.

3. Conclusion

We have investigated the effect of different end groups on BCP self-assembly in solution. BCPs with hydroxyl, methoxy, azido, and amino groups at the end of the hydrophilic PEG block self-assembled into different morphologies ranging from vesicles to hexosomes under the same self-assembly conditions. Based on the packing parameter (p) analogy, we speculate that the interactions between the end groups and a common solvent (acetone and dioxane) or water could determine the headgroup area (a_0) of the BCPs in solution, leading to the different self-assembly behaviors. Interestingly, different junctions between two blocks such as amide and triazole units also resulted in the self-assembly of different morphologies. This was attributed to the hydrogen bonding capability or the different lengths of the junctions. In summary, we have demonstrated that the end groups and junction, which account for a very small portion of an entire BCP, can significantly influence the BCP self-assembly. We envision that our findings will provide new insights to control the self-assembly of block copolymers.

Conflicts of interest

There are no conflicts of interest to declare.

Acknowledgements

We acknowledge supports from the National Research Foundation (NRF) of Korea (2019R1A2C3007541), the Technology Innovation Program (or Industrial Strategic Technology Development Program-Alchemist Project) (20012390, 4D Molecular-Nano-Addressable Lithographic Self-Assembly (4D MONALISA)) funded by the Ministry of Trade, Industry & Energy (MOTIE, Korea), and Creative-Pioneering Researchers Programs (30520190050) by Seoul National University (SNU).

Notes and references

1 J. C. M. van Hest, D. A. P. Delnoye, M. W. P. L. Baars, M. H. P. van Genderen and E. W. Meijer, *Science*, 1995, **268**, 1592–1595.
2 D. E. Discher and A. Eisenberg, *Science*, 2002, **297**, 967–973.
3 A. Blanazs, S. P. Armes and A. J. Ryan, *Macromol. Rapid Commun.*, 2009, **30**, 267–277.
4 Y. Mai and A. Eisenberg, *Chem. Soc. Rev.*, 2012, **41**, 5969–5985.
5 U. Tritschler, S. Pearce, J. Gwyther, G. R. Whittell and I. Manners, *Macromolecules*, 2017, **50**, 3439–3463.
6 Y. La, C. Park, T. J. Shin, S. H. Joo, S. Kang and K. T. Kim, *Nat. Chem.*, 2014, **6**, 534–541.
7 H. Yu, X. Qiu, S. P. Nunes and K.-V. Peinemann, *Nat. Commun.*, 2014, **5**, 4110.
8 T. H. An, Y. La, A. Cho, M. G. Jeong, T. J. Shin, C. Park and K. T. Kim, *ACS Nano*, 2015, **9**, 3084–3096.
9 Y. La, T. H. An, T. J. Shin, C. Park and K. T. Kim, *Angew. Chem., Int. Ed.*, 2015, **54**, 10483–10487.
10 Z. Lin, S. Liu, W. Mao, H. Tian, N. Wang, N. Zhang, F. Tian, L. Han, X. Feng and Y. Mai, *Angew. Chem., Int. Ed.*, 2017, **56**, 7135–7140.
11 X. Lyu, A. Xiao, W. Zhang, P. Hou, K. Gu, Z. Tang, H. Pan, F. Wu, Z. Shen and X.-H. Fan, *Angew. Chem., Int. Ed.*, 2018, **57**, 10132–10136.
12 Y. La, J. Song, M. G. Jeong, A. Cho, S.-M. Jin, E. Lee and K. T. Kim, *Nat. Commun.*, 2018, **9**, 5327.
13 S. Ha and K. T. Kim, *Polym. Chem.*, 2019, **10**, 5805–5813.
14 J. Kim, M. Yoon, S.-M. Jin, J. Lee, Y. La, E. Lee and K. T. Kim, *Polym. Chem.*, 2019, **10**, 3778–3785.
15 H.-K. Liu, L.-J. Ren, H. Wu, Y.-L. Ma, S. Richter, M. Godehardt, C. Kübel and W. Wang, *J. Am. Chem. Soc.*, 2019, **141**, 831–839.
16 X. Liu and I. Gitsov, *Macromolecules*, 2019, **52**, 5563–5573.
17 Y. Sun, J. Kim and K. T. Kim, *RSC Adv.*, 2019, **9**, 25423–25428.
18 S. Ha, Y. La and K. T. Kim, *Acc. Chem. Res.*, 2020, **53**, 620–631.
19 H. Ma and K. T. Kim, *Macromolecules*, 2020, **53**, 711–718.
20 L. Zhang, C. Bartels, Y. Yu, H. Shen and A. Eisenberg, *Phys. Rev. Lett.*, 1997, **79**, 5034–5037.
21 A. L. Parry, P. H. H. Bomans, S. J. Holder, N. A. J. M. Sommerdijk and S. C. G. Biagini, *Angew. Chem., Int. Ed.*, 2008, **47**, 8859–8862.
22 B. E. McKenzie, F. Nudelman, P. H. H. Bomans, S. J. Holder and N. A. J. M. Sommerdijk, *J. Am. Chem. Soc.*, 2010, **132**, 10256–10259.
23 S. J. Holder and N. A. J. M. Sommerdijk, *Polym. Chem.*, 2011, **2**, 1018–1028.
24 B. E. Mckenzie, S. J. Holder and N. A. J. M. Sommerdijk, *Curr. Opin. Colloid Interface Sci.*, 2012, **17**, 343–349.
25 B. E. McKenzie, J. F. de Visser, H. Friedrich, M. J. M. Wirix, P. H. H. Bomans, G. de With, S. J. Holder and N. A. J. M. Sommerdijk, *Macromolecules*, 2013, **46**, 9845–9848.
26 B. E. McKenzie, H. Friedrich, M. J. M. Wirix, J. F. de Visser, O. R. Monaghan, P. H. H. Bomans, F. Nudelman, S. J. Holder and N. A. J. M. Sommerdijk, *Angew. Chem., Int. Ed.*, 2015, **54**, 2457–2461.
27 B. E. McKenzie, J. F. de Visser, G. Portale, D. Hermida-Merino, H. Friedrich, P. H. H. Bomans, W. Bras, O. R. Monaghan, S. J. Holder and N. A. J. M. Sommerdijk, *Soft Matter*, 2016, **12**, 4113–4122.
28 H. He, K. Rahimi, M. Zhong, A. Mourran, D. R. Luebke, H. B. Nulwala, M. Möller and K. Matyjaszewski, *Nat. Commun.*, 2017, **8**, 14057.

29 K. E. B. Doncom, L. D. Blackman, D. B. Wright, M. I. Gibson and R. K. O'Reilly, *Chem. Soc. Rev.*, 2017, **46**, 4119–4134.
30 C. K. Wong, X. Qiang, A. H. E. Müller and A. H. Gröschel, *Prog. Polym. Sci.*, 2020, **102**, 101211.
31 J. Xu, L. Tao, C. Boyer, A. B. Lowe and T. P. Davis, *Macromolecules*, 2011, **44**, 299–312.
32 J. Du, H. Willcock, J. P. Patterson, I. Portman and R. K. O'Reilly, *Small*, 2011, **7**, 2070–2080.
33 T. Liu, W. Tian, Y. Zhu, Y. Bai, H. Yan and J. Du, *Polym. Chem.*, 2014, **5**, 5077–5088.
34 G. Jo, H. Ahn and M. J. Park, *ACS Macro Lett.*, 2013, **2**, 990–995.
35 G. Jo, O. Kim, H. Kim, U. Hyeok Choi, S.-B. Lee and M. Jeong Park, *Polym. J.*, 2016, **48**, 465–472.
36 H. Y. Jung, P. Mandal, G. Jo, O. Kim, M. Kim, K. Kwak and M. J. Park, *Macromolecules*, 2017, **50**, 3224–3233.
37 J. Kim, H. Y. Jung and M. J. Park, *Macromolecules*, 2020, **53**, 746–763.
38 L. D. Blackman, K. E. B. Doncom, M. I. Gibson and R. K. O'Reilly, *Polym. Chem.*, 2017, **8**, 2860–2871.
39 S. Y. Khor, N. P. Truong, J. F. Quinn, M. R. Whittaker and T. P. Davis, *ACS Macro Lett.*, 2017, **6**, 1013–1019.
40 M. Grzelakowski and K. Kita-Tokarczyk, *Nanoscale*, 2016, **8**, 6674–6683.
41 H. Che, L. N. J. de Windt, J. Zhu, I. A. B. Pijpers, A. F. Mason, L. K. E. A. Abdelmohsen and J. C. M. van Hest, *Chem. Commun.*, 2020, **56**, 2127–2130.
42 K. Matyjaszewski, Y. Nakagawa and S. G. Gaynor, *Macromol. Rapid Commun.*, 1997, **18**, 1057–1066.
43 R. R. Karimov, A. Sharma and J. F. Hartwig, *ACS Cent. Sci.*, 2016, **2**, 715–724.
44 J. C. Foster, S. Varlas, B. Couturaud, J. R. Jones, R. Keogh, R. T. Mathers and R. K. O'Reilly, *Angew. Chem., Int. Ed.*, 2018, **57**, 15733–15737.
45 S. Varlas, J. C. Foster, L. A. Arkinstall, J. R. Jones, R. Keogh, R. T. Mathers and R. K. O'Reilly, *ACS Macro Lett.*, 2019, **8**, 466–472.
46 J. C. Foster, I. Akar, M. C. Grocott, A. K. Pearce, R. T. Mathers and R. K. O'Reilly, *ACS Macro Lett.*, 2020, **9**, 1700–1707.
47 Y. Hua and A. H. Flood, *Chem. Soc. Rev.*, 2010, **39**, 1262–1271.
48 D.-Y. Wang, L.-Y. You, J.-L. Wang, H. Wang, D.-W. Zhang and Z.-T. Li, *Tetrahedron Lett.*, 2013, **54**, 6967–6970.
49 M. R. Molla and S. Ghosh, *Chem.–Eur. J.*, 2012, **18**, 9860–9869.
50 P. Rajdev, M. R. Molla and S. Ghosh, *Langmuir*, 2014, **30**, 1969–1976.
51 A. Sikder, A. Das and S. Ghosh, *Angew. Chem., Int. Ed.*, 2015, **54**, 6755–6760.
52 A. Sikder, D. Ray, V. K. Aswal and S. Ghosh, *Angew. Chem., Int. Ed.*, 2019, **58**, 1606–1611.
53 A. Sikder, Y. Xie, M. Thomas, M. J. Derry and R. K. O'Reilly, *Nanoscale*, 2021, **13**, 20111–20118.
54 Y. Luo, D. Montarnal, N. J. Treat, P. D. Hustad, M. D. Christianson, E. J. Kramer, G. H. Fredrickson and C. J. Hawker, *ACS Macro Lett.*, 2015, **4**, 1332–1336.
55 Q. Zhang, J. Lin, L. Wang and Z. Xu, *Prog. Polym. Sci.*, 2017, **75**, 1–30.